Journal of Petroleum Science and Engineering 77 (2011) 183–188

Contents lists available at ScienceDirect

Journal of Petroleum Science and Engineering

journal homepage: www.elsevier.com/locate/petrol

Analyses of stress strain behavior and constitutive model of artificial methane hydrate

Feng Yu, Yongchen Song *, Weiguo Liu, Yanghui Li, Weihaur Lam

Key Laboratory of Ocean Energy Utilization and Energy Conservation of Ministry of Education, Dalian University of Technology, Dalian 116024, China

ARTICLE INFO

Article history:
Received 8 July 2010
Accepted 28 March 2011
Available online 6 April 2011

Keywords:
triaxial
stress strain behavior
constitutive model
methane hydrate

ABSTRACT

In this paper, a low-temperature high-pressure triaxial test system including pressure crystal device (sample preparation system) was developed, in which the conditions of hydrate stabilized can be maintained. To determine the stress strain behavior of methane hydrate, the triaxial shear tests were performed under the condition of strain rates of 1.5%/min, temperatures $\theta = -5, -10$, and -20 °C and confining pressures $P = 2.5$, 5 and 10 MPa. The preliminary results show that the stress strain curves can be divided into two stages: the rapid structural damage stage and the complete structural damage stage (or the yield stage). Based on the experimental and analysis results of stress strain behavior of triaxial tests, this paper proposes a modified nonlinear elastic Duncan–Chang constitutive model suitable for artificial methane hydrate. The modified model takes into account the effect of temperature and confining pressure as well as hydrate structure on the stress strain behavior. By comparing experimental with simulation results, the validity of model had been evaluated.

1. Introduction

Methane hydrate has been considered as one of the most promising new energies to alleviate the energy crisis by many researchers (Collett et al., 1998; Kvenvolden, 1988; Kvenvolden and Lorenson, 2001). The existence of a large amount of methane hydrate in the permafrost and ocean sediment has been estimated worldwide (Alexei, 2004; Gornitz and Fung, 1994). At present the exploitation of methane hydrate has been investigated widely, the promising methods for dissociation of methane hydrate are thought to be "depressurization", "thermal injection" and "usage of inhibitors" in production wells (George and Timothy, 2003; Pooladi-Darvish, 2004). However, the dissociation of methane hydrate during drilling for exploration and production may result in seabed subsidence and deformation of methane hydrate sediment strata (Brown et al., 2006; Glasby, 2003; MacDonald et al., 1994). In order to analyze exploitation safety and slope stability of hydrate reservoir, it is important to study mechanical properties of methane hydrate and develop the constitutive model.

At present, the low-temperature high-pressure triaxial testing apparatus was widely developed to determine mechanical behavior of hydrate or hydrate-bearing sediment. Because hydrate reservoir deposits are under the ground surface or sea floor at depths of hundreds meters or even a thousand meters, it is very hard and expensive for the triaxial tests to drill the cores of natural hydrate. In view of this, most of hydrate samples for triaxial tests are made of methane and water or ice under laboratory conditions. Hyodo et al. (2002) used methane and water as raw materials to manufacture the methane hydrate. The researchers showed that the strength of methane hydrate increased at low temperatures and high pressures. Moreover, the hydrate-bearing sediments were made with methane being fed into the aquiferous pore medium at constant pressure. The shear strength of artificial hydrate-bearing sediments was similar to that of natural hydrate-bearing sediments (Masui et al., 2008; Winters et al., 2004), and the strength also varied with the content of hydrate and sediment properties as well as experimental conditions (Hyodo et al., 2005; Masui et al., 2005; Winters et al., 2007). Furthermore, during hydrate dissociation without axial loading, the volumetric strain has dilative tendency whether there is the decrease of the effective confining pressure or not (Hyodo et al., 2007). The physical chemical properties of tetrahydrofuran hydrate are similar to that of methane hydrate, thus methane hydrate can be substituted with tetrahydrofuran hydrate which forms more easily. These researches also reflected mechanical behavior of methane hydrate to some extent (Lu et al., 2008; Yun et al., 2007). Subsequently, based on experimental results of triaxial tests of Toyoura sand containing synthetic methane hydrate, Masui et al. developed a variable-compliance-type constitutive model to formulate stress–strain relationship (Miyazaki et al., 2008). The model took into account the time-dependent property which was influenced by the methane hydrate saturation and effective confining pressure.

Although there have been a few researches on the physical chemical and mechanical properties of methane hydrate, the mechanical behavior doesn't have to be fully and deeply investigated

* Corresponding author. Tel.: +86 411 84706008; fax: +86 411 84708015.
E-mail address: songyc@dlut.edu.cn (Y. Song).

0920-4105/$ – see front matter © 2011 Elsevier B.V. All rights reserved.
doi:10.1016/j.petrol.2011.03.004

Table 1
Experimental condition and number of triaxial tests on methane hydrate.

Temperature (°C)	Confining pressure σ (MPa)	Number of tests under strain rate (1.5%/min)	Total number of tests
	2.5	3	10
−5	5	2	
	10	3	
	2.5	2	7
−10	5	3	
	10	2	
	2.5	2	7
−20	5	3	
	10	2	

yet. Moreover, few studies have been done on the constitutive model of hydrate to analyze stress strain behavior. Therefore in this paper a triaxial testing equipment with low temperature and high pressure was developed to determine and analyze the mechanical behavior of artificial methane hydrate in various conditions. Furthermore, the constitutive model suitable for artificial methane hydrate was established on the basis of nonlinear elastic Duncan–Chang model (Duncan and Chang, 1970; Wang et al., 2004a).

2. Experimental program

Table 1 summarizes the testing matrix for the parametric study on triaxial compression behavior of methane hydrate. Tests were carried out in the condition of temperature $\theta = -5, -10, -20$ °C and confining pressure $P = 2.5, 5, 10$ MPa. The strain rate was used: 1.5%/min. To check the validity of the experimental results, the identical testing conditions were repeated at least once.

2.1. Triaxial testing system

The schematic diagram of triaxial testing system used is shown in Fig. 1. Confining pressure was provided up to 30 MPa by a closed-loop pressure control servo-system which is capable of continuously maintaining a set cell pressure. The pressure control servo-system consists of a computer control unit, a digital control servomotor and a hydraulic piston. The computer control unit directly compares the actual cell pressure with the target pressure, and sends a correction signal to the servomotor. Then the servomotor controls the hydraulic piston to advance or retract in order to drive the actual cell pressure to reach the target pressure. In temperature control-system the temperature is adjusted range from −30 to 25 °C using a controllable constant temperature bath and heat exchangers. The temperature of liquid coolant in the constant temperature bath always maintains a few degrees lower than the desired testing temperature. When the actual cell temperature is higher than the target temperature, the digital control circulating pump drives liquid coolant into heat exchanger to cool cell down. The axial strain rate is controlled by an axial loading frame. This loading frame can apply 60 KN loading capacity for specimen.

2.2. Testing procedures

The methane hydrate for this study was manufactured in the reactor using methane and ice powder as raw materials. The ice powder was broken by the block shaving machine in advance, and was filled into the reactor. The high pressure methane gas was also injected into the closed reactor. Then the reactor was put in the refrigerator for forming methane hydrate in the low temperature. After the formation reaction was completed, the methane hydrate was removed from the reactor and put into a mold to make specimen at high pressure (10 MPa) using pressure crystal device. Finally the specimens were removed from the mold, wrapped in rubber membrane and timely put in the pressure chamber. Prior to shearing, the cell pressure and temperature were adjusted to gain the desired experimental condition. All tests including specimen preparation were carried out in low temperature cold storage (−10 °C).

3. Stress strain behavior of methane hydrate

Pressure and temperature play important roles in studying the physical chemical and mechanical properties of methane hydrate. Methane hydrate can keep long-term stability only in the conditions of low temperature and high pressure. Moreover, pressure and temperature not only affect the formation or dissociation of methane hydrate, but also decide the stress strain behavior.

Fig. 2 shows the axial strain-dependence curves of deviator stress under identical temperature and strain rate at the confining pressure of 2.5, 5 and 10 MPa respectively, and Fig. 3 shows the axial strain-dependence curves of deviator stress under identical confining pressure at temperatures of −5, −10 and −20 °C respectively. It can be seen that the stress strain curves all appeared to be of hyperbolical shape under

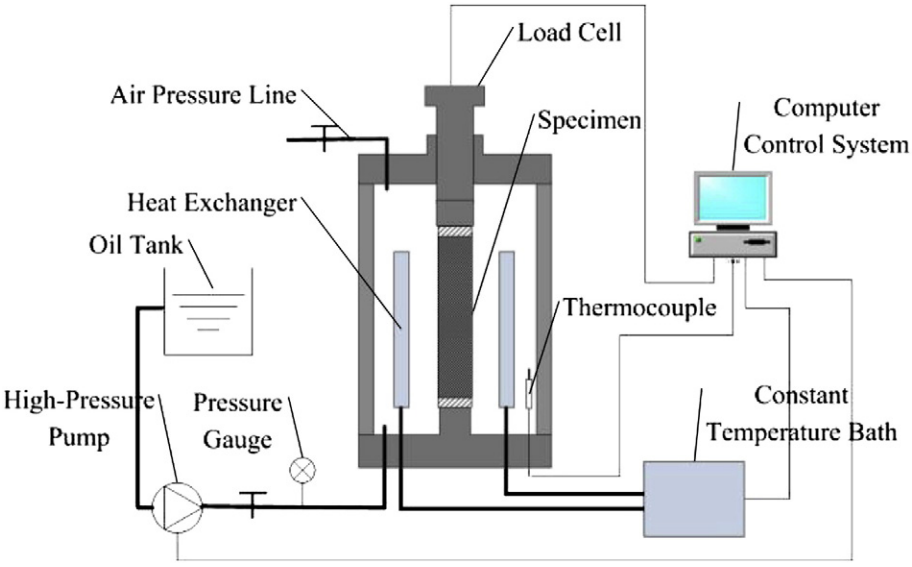

Fig. 1. Schematic diagram of triaxial testing system.

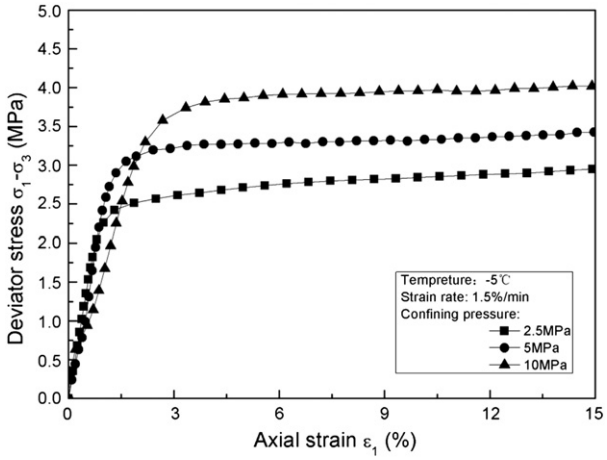

Fig. 2. The axial strain-dependence curves of deviator stress under different confining pressure.

different confining pressures and temperatures. Furthermore, the lower the temperature was or the higher the pressure was, the larger the peak deviator stress became. This mechanical property of methane hydrate is similar with that of the soil. Consequently, according to the research method on the soil stress–strain behavior and structure the stress–strain curves of methane hydrate can be divided into two stages: the rapid structural damage stage and the complete structural damage stage. At the rapid structural damage stage the deviator stress rapidly increased with the increasing axial deformation from initial strain up to about 2%, and the structure of methane hydrate also rapidly was damaged. When the specimens reached the complete structural damage stage at the large strains beyond 2%, the axial deformation presented an overwhelming increase with the continuous load. However, the deviator stress had almost no increase. In fact, the structure of specimen had already been damaged completely and the specimen had approached or reached failure state.

4. Constitutive model

Although some progress of the mechanical properties was made by many researchers, the reasonable constitutive model hardly was established to predict stress strain behavior of methane hydrate. Based on the data of the triaxial tests, the relationship between the deviator principal stress and the strain for methane hydrate is shown in Figs. 2 and 3. As mentioned above, the stress strain curves appeared to be of hyperbolical shape. According to the nonlinear elastic Duncan–Chang model, the corresponding expression for the hyperbolic stress–strain function is given by:

$$\sigma_1-\sigma_3=\frac{\varepsilon_1}{a+b\varepsilon_1} \tag{1}$$

in which: σ_1–σ_3 is the deviator stress, ε_1 is the axial strain corresponding to the deviator stress, and a and b are the experimental coefficients. Eq. (1) can be transformed into the following form:

$$\frac{\varepsilon_1}{\sigma_1-\sigma_3}=a+b\varepsilon_1. \tag{2}$$

Consequently, a is the intercept on the vertical axis of $\varepsilon_1/(\sigma_1$–$\sigma_3)$, and b is the slope of the straight line of $\varepsilon_1/(\sigma_1$–$\sigma_3)$~ε_1. Fig. 4 shows that the triaxial test data of methane hydrate were processed in accordance with the relationship of $\varepsilon_1/(\sigma_1$–$\sigma_3)$~ε_1. It can be seen that the experimental points from initial strain up to about 2% strain (first stage) deviated from the straight line. This phenomenon which often happens is ignored for the triaxial tests of soil. Therefore, the relationship of $\varepsilon_1/(\sigma_1$–$\sigma_3)$~ε_1 explained later will not be processed temporarily at first stage. According to Eq. (2), the values of a and b which are related to the pressure and temperature are given in Table 2 at second stage of the line $\varepsilon_1/(\sigma_1$–$\sigma_3)$~ε_1 for the triaxial tests of methane hydrate.

According to Eq. (1), when ε_1 approaches zero the initial tangent modulus E_i of the stress strain curves can be obtained by the following:

$$E_i=\frac{1}{a}. \tag{3}$$

It shows that a represents the reciprocal of initial tangent modulus E_i When ε_1 approaches infinity, the ultimate deviator stress $(\sigma_1$–$\sigma_3)_{ult}$ can be derived by the following:

$$(\sigma_1-\sigma_3)_{ult}=\frac{1}{b} \tag{4}$$

or

$$b=\frac{1}{(\sigma_1-\sigma_3)_{ult}}. \tag{5}$$

It can be seen that b represents the reciprocal of the ultimate deviator stress $(\sigma_1$–$\sigma_3)_{ult}$ corresponding to the hyperbolic asymptote.

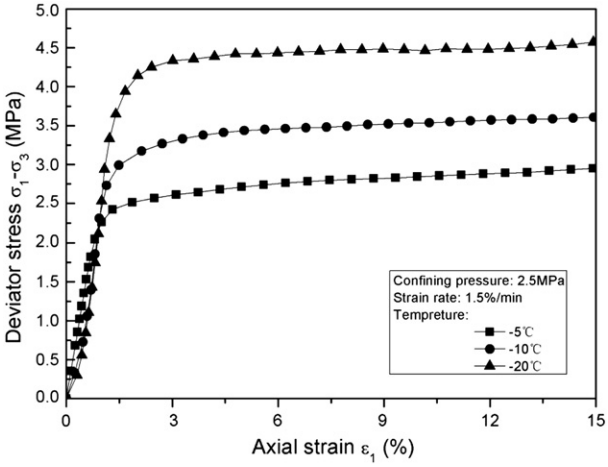

Fig. 3. The axial strain-dependence curves of deviator stress under different temperatures.

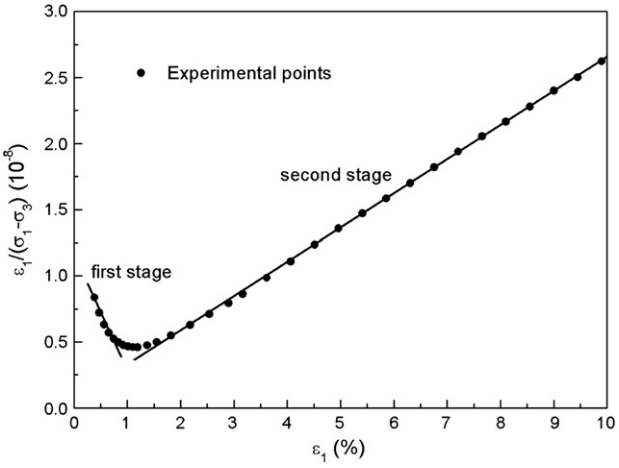

Fig. 4. The relationship of $\varepsilon_1/(\sigma_1$–$\sigma_3)$~ε_1.

Table 2
Values of the coefficients of a and b at the second stage.

$\sigma_3\backslash\theta$	−5 °C		−10 °C		−20 °C	
Coefficients	a	b	a	b	a	b
2.5 MPa	2.01×10^{-9}	3.28×10^{-7}	1.06×10^{-9}	2.71×10^{-7}	5.52×10^{-10}	2.16×10^{-7}
5 MPa	1.15×10^{-9}	2.85×10^{-7}	8.40×10^{-10}	2.55×10^{-7}	4.21×10^{-10}	1.87×10^{-7}
10 MPa	9.8×10^{-9}	2.41×10^{-7}	7.96×10^{-10}	2.11×10^{-7}	4.21×10^{-10}	1.62×10^{-7}

According to Eqs. (3) and (4), the values of E_{i2} and $(\sigma_1-\sigma_3)_{ult2}$ at the second stage are given in Table 3.

Fig. 5 shows the confining pressure-dependence curves of initial tangent modulus E_i under different temperatures. It can be seen that the E_i–σ_3 curve change tendency is almost kept consistent with the increasing confining pressure under different temperatures. Based on the curve change tendency, E_i is defined as a power function of confining pressure σ_3 in the Duncan–Chang hyperbola model.

$$E_i = Kp_a\left(\frac{\sigma_3}{p_a}\right)^n \tag{6}$$

in which, K and n are experimental constants. However, The Duncan–Chang model only considers the effect of the confining pressure on the initial tangent modulus E_i. From Fig. 5E_{i2} increased with not only the increasing confining pressure but also the decreasing temperature. Thus for methane hydrate E_i can be redefined in the following form:

$$E_i = e^{c_0 + c_1\theta}p_a\left(\frac{\sigma_3}{p_a}\right)^{c_2 + c_3\theta} \tag{7}$$

in which, P_a is atmospheric pressure (P_a= 101.4kPa), θ is temperature (°C) and c_0, c_1, c_2 and c_3 are experimental constants. According to the data of E_{i2} in Table 2, E_{i2} can be obtained in the form below:

$$E_{i2} = e^{6.56-0.142\theta}p_a\left(\frac{\sigma_3}{p_a}\right)^{0.522 + 0.0186\theta}. \tag{8}$$

Fig. 6 shows the confining pressure-dependence curves of ultimate deviator stress $(\sigma_1-\sigma_3)_{ult2}$ under different temperatures. The curves all presented a good linear relationship with confining pressure. Moreover they were almost parallel to each other. Thus the function expression for $(\sigma_1-\sigma_3)_{ult2}$ is written:

$$(\sigma_1-\sigma_3)_{ult2} = A_0 + A_1\sigma_3. \tag{9}$$

A_0 and A_1 are the intercept and the slope of the curve under each temperature. In addition, it was found that the values of A_0 and A_1 varied linearly with temperature. Therefore the expression is given by:

$$A_0 = 2.265-0.0984\theta \tag{10}$$

$$A_1 = 0.1154-0.004\theta. \tag{11}$$

By substituting the confining pressure σ_3 and the temperature θ into Eqs. (8)–(11), the initial tangent modulus E_{i2} and the ultimate deviator stress $(\sigma_1-\sigma_3)_{ult2}$ can be calculated. Furthermore, the values of a and b can be obtained from Eqs. (3) and (5), respectively. So the stress–strain behavior under the axial loading will be predicted. Some experimental and calculated stress strain curves of the specimens of methane hydrate were shown in Fig. 7. It can be seen that the predicted stress strain curves match the experimental stress strain curves well at the temperatures of –5 °C and the pressure of 2.5, 5 MPa.

However, there were some differences between the predicted and experimental stress strain behaviors at small strains at the temperature of −20 °C although the peak deviator stress was almost the same for both the model and test. The deviator stress increased with the axial strain more slowly for the test than for the model at small strains. This may be due to differences in the relationship of $\varepsilon_1/(\sigma_1-\sigma_3)\sim\varepsilon_1$ between small strains (first stage) and large strain (second stage) in Fig. 4. The small strain stage is just the rapid structural damage stage mentioned above. Both the of stages shown in Fig. 4 correspond to the rapid structural damage stage and the complete structural damage stage. Therefore the stress strain behavior also can be divided into two stages. Based on the structure of methane hydrate, the damage ratio ω is introduced into the initial modified model above. The expression of modified model containing the damage ratio ω is given by:

$$\sigma_1-\sigma_3 = \frac{\varepsilon_1}{\frac{1}{(1-\omega)E_{i1} + \omega E_{i2}} + \frac{\varepsilon_1}{(1-\omega)(\sigma_1-\sigma_3)_{ult1} + \omega(\sigma_1-\sigma_3)_{ult2}}}. \tag{12}$$

in which, E_{i1} and $(\sigma_1-\sigma_3)_{ult1}$ are the initial tangent modulus and ultimate deviator stress at the first stage. According to the above derivation method on initial tangent modulus E_i, E_{i1} is given by:

$$E_{i1} = e^{8.88-0.0871\theta}p_a\left(\frac{\sigma_3}{p_a}\right)^{-0.271-0.007\theta}. \tag{13}$$

Table 3
Values of the parameters of E_{i2} and $(\sigma_1-\sigma_3)_{ult2}$ at the second stage.

$\sigma_3\backslash\theta$	−5 °C		−10 °C		−20 °C	
Parameters	E_{i2} (Pa)	$(\sigma_1-\sigma_3)_{ult2}$ (Pa)	E_{i2} (Pa)	$(\sigma_1-\sigma_3)_{ult2}$ (Pa)	E_{i2} (Pa)	$(\sigma_1-\sigma_3)_{ult2}$ (Pa)
2.5 MPa	4.98×10^8	3.05×10^6	9.43×10^8	3.70×10^6	1.82×10^9	4.63×10^6
5 MPa	8.70×10^8	3.51×10^6	1.19×10^9	3.92×10^6	2.38×10^9	5.35×10^6
10 MPa	1.02×10^9	4.15×10^6	1.25×10^9	4.74×10^6	2.38×10^9	6.17×10^6

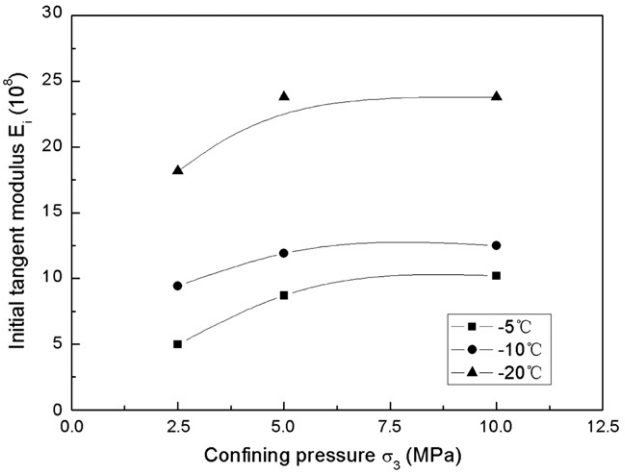

Fig. 5. The confining pressure-dependence curves of initial tangent modulus Ei2 under different temperatures.

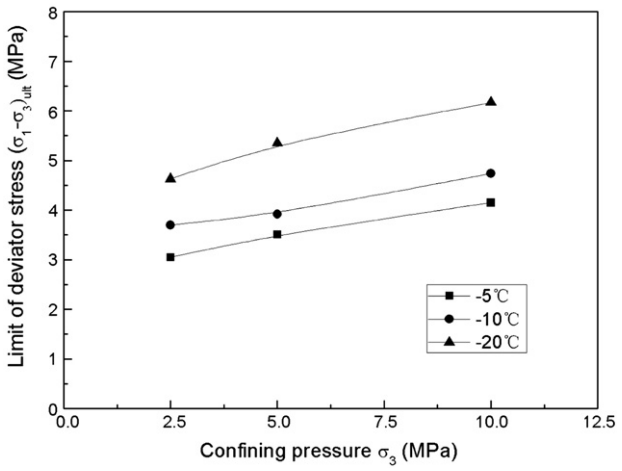

Fig. 6. The confining pressure-dependence curves of ultimate deviator stress $(\sigma_1-\sigma_3)_{ult2}$ under different temperatures.

The values of the coefficient b at the first stage from the triaxial tests are negative. It just represents the slope of the straight line at the first stage. Although the ultimate deviator stress $(\sigma_1-\sigma_3)_{ult1}$ is equal to the reciprocal of b, it doesn't represent the ultimate deviator stress of stress strain curve and has no definite physical meaning. The $(\sigma_1-\sigma_3)_{ult1}$ only increased with the decrease of temperature, but was independent of confining pressure. $(\sigma_1-\sigma_3)_{ult1}$ is given by:

$$(\sigma_1-\sigma_3)_{ult1} = \frac{1}{0.047\theta + 0.144}. \tag{14}$$

The elastic–plastic damage model established by Shen (1993) proposed a damage ratio function of strain. But the function parameters need be determined by the unconfined compression tests, which make the experimental method complicated. Therefore this study uses the simplified the damage ratio function suggested by Wang et al. (2004b).

$$\omega = 1-e^{-B\varepsilon_1/(\varepsilon_{lu}-\varepsilon_1)} \tag{15}$$

in which, ε_{lu} is the maximum principal strain corresponding to the soil failure, which is equal to 0.15 for strain hardening. B is the experimental parameter which is equal to 15 in the Wang's model. However, it was found that B was no longer a constant for the hydrate tests. It varied with confining pressure and temperature.

$$B = 36.5-0.942\sigma_3 + 0.7\theta \tag{16}$$

The input parameters for the model prediction had been obtained. According to Eq. (12) the modified model containing damage ratio ω was then used to predict the stress strain behavior at the temperatures of −10 and −20 °C. Fig. 8 presents the model predictions as well as the experimental results from the hydrate tests. It can be seen that the calculated stress strain curves match the experimental stress strain curves well not only at small strains but also at large strains. The results indicate that the modified Duncan–Chang model can be used to simulate the stress strain behavior of methane hydrate under triaxial tests.

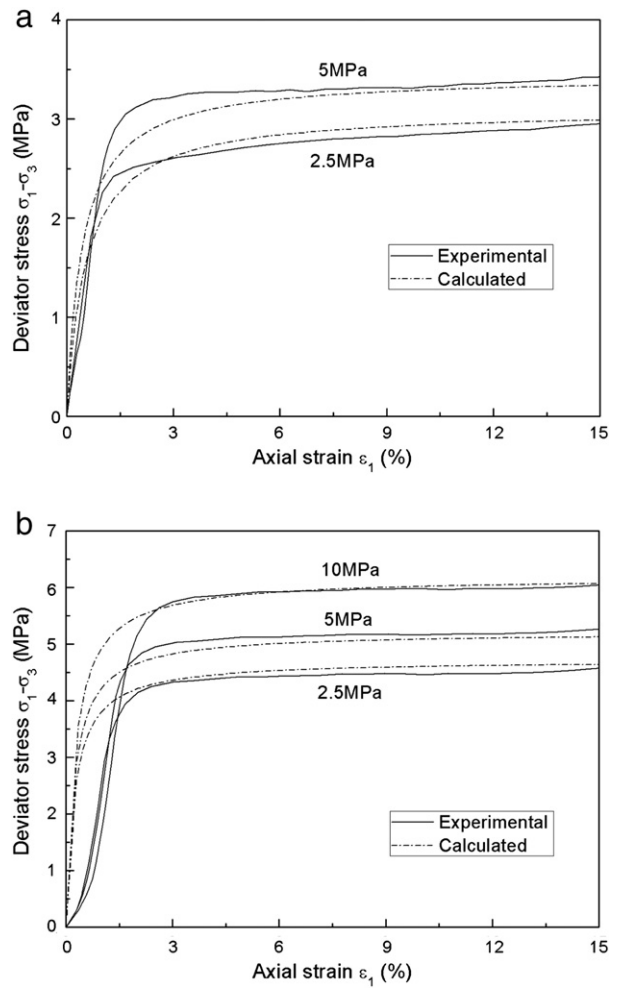

Fig. 7. Experimental and calculated stress–strain curves at the temperatures of −5 °C (a) and −20 °C (b).

5. Conclusions

Using A high-pressure low-temperature triaxial system, the experimental study on the stress strain behavior of methane hydrate was made. Based on this, the modified Duncan–Chang constitutive model suitable for methane hydrate was presented. By analyzing the experimental and simulation results, the following conclusions can be drawn.

The triaxial shear tests indicate that the curve of stress strain can be divided into two different stages of deformation: the rapid structural damage stage and the complete structural damage stage. The deviator stress rapidly increased with the increasing axial deformation at the rapid structural damage stage, and had almost no increase at the complete structural damage stage. The peak deviator stress of methane hydrate increased in condition of the enhancement of confining pressure and the decrease of temperature.

The linear relationship of $\varepsilon_1/(\sigma_1-\sigma_3)\sim\varepsilon_1$ can be divided into two different stages corresponding to the rapid structural damage stage and the complete structural damage stage. At first stage the initial tangent modulus E_{i1} increased with the increasing confining pressure and the decreasing temperature, and the ultimate deviator stress $(\sigma_1-\sigma_3)_{ult1}$ only varied with temperature. However, at second stage the decreasing temperature and increasing confining pressure both caused the increase of the initial tangent modulus E_{i2} and ultimate deviator stress $(\sigma_1-\sigma_3)_{ult2}$. In view of this, the stress strain behavior also can be divided into two stages, and the damage ratio ω was introduced into the modified model.

Using a relatively simple constitutive model, modifications were made to describe mechanical behaviors of methane hydrate. Furthermore, experimental and simulation results were compared. When the temperature was more than −5°C and confining pressure was less than 5 MPa, the predicted stress strain curves of methane hydrate

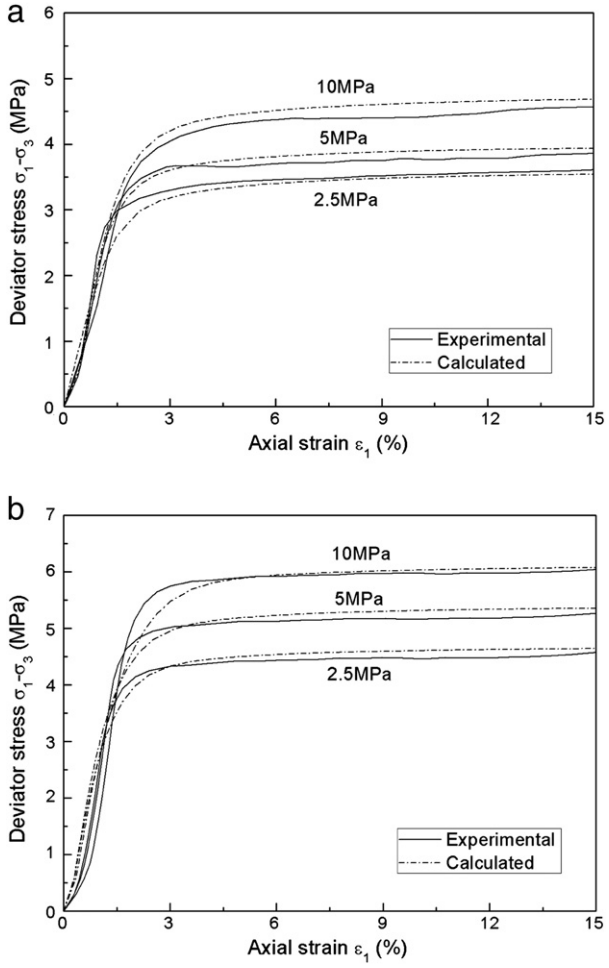

Fig. 8. Experimental and calculated stress–strain curves at the temperatures of −10 °C (a) and −20 °C (b).

matched the experimental stress strain curves well using the initial modified Duncan–Chang model. When the temperature was less than −10 °C, the modified model containing damage ratio ω was suitable for predicting the stress strain behavior. This may be due to differences in the relationship of $\varepsilon_1/(\sigma_1-\sigma_3)\sim\varepsilon_1$ between small strains and large strain. However, the differences hardly had the effect on validity of initial modified model prediction in the condition of higher temperature and lower confining pressure.

Nomenclature

θ	temperature (°C)
P	pressure (MPa)
P_a	atmospheric pressure
ε_1	axial strain (%)
ε_{lu}	maximum principal strain corresponding to the soil failure
σ_3	confining pressure (MPa)
$\sigma_1-\sigma_3$	deviator stress (MPa)
$(\sigma_1-\sigma_3)_{ult}$	ultimate deviator stress (Pa)
$(\sigma_1-\sigma_3)_{ult1}$	ultimate deviator stress at the first stage (Pa)
$(\sigma_1-\sigma_3)_{ult2}$	ultimate deviator stress at the second stage (Pa)
E_i	initial tangent modulus (Pa)
E_{i1}	initial tangent modulus at the first stage (Pa)
E_{i2}	initial tangent modulus at the second stage (Pa)
ω	damage ratio
a	intercept on the vertical axis
b	slope of the straight line
K	experimental constants
n	experimental constants
c_0	experimental constants
c_1	experimental constants
c_2	experimental constants
c_3	experimental constants
A_0	intercept of the curve
A_1	slope of the curve
B	experimental parameter

Acknowledgments

The project is supported by the National Science and Technology Major Project, China (Grant No. 2008ZX05026-04-010), the China National High Technology Research and Development (863) Program (Grant No. 2006AA09A209-5), and the Key Program of National Natural Science Foundation of China (50736001).

References

Alexei, V.M., 2004. Global estimates of hydrate-bound gas in marine sediments: how much is really out there? Earth Sci. Rev. 66, 183–197.
Brown, H.E., Holbrook, W.S., Hornbach, M.J., Nealon, J., 2006. Slide structure and role of gas hydrate at the northern boundary of the Storegga Slide, offshore Norway. Mar. Geology 229 (3–4), 179–186.
Collett, T.S., Kuuskraa, V.A., Arlington, V.A., 1998. Hydrates contain vast store of world gas resources. Oil Gas J. 96 (19), 90–95.
Duncan, J.M., Chang, C.Y., 1970. Nonlinear analysis of stress and strain in soils. J. Soil Mech. Foundations Division ASCE 1629–1654.
George, J.M., Timothy, S.C., 2003. Strategies for gas production from hydrate accumulations under various geological and reservoir conditions. Proceedings, TOUGH Symposium 2003, Berkeley.
Glasby, G.P., 2003. Potential impact on climate of the exploitation of methane hydrate deposits offshore. Mar. Petroleum Geology 20, 163–175.
Gornitz, V., Fung, I., 1994. Potential distribution of methane hydrates in the world's oceans. Glob. Biogeochemical 8 (3), 335–347.
Hyodo, M., Hyde, A.F.L., Nakata, Y., Yoshimoto, N., Fukunaga, M., Kubo, K., Nanjo, Y., Matsuo, T., Nakamura, K., 2002. Triaxial compressive strength of methane hydrate. Proceedings of the 12th International Offshore and Polar Engineering Conference, ISOPE, pp. 422–428.
Hyodo, M., Nakata, Y., Yoshimoto, N., Ebinuma, T., 2005. Basic research on the mechanical behavior of methane hydrate-sediments mixture. J. Jpn. Geotechnical Soc. Soils Foundations 45 (1), 75–85.
Hyodo, M., Nakata, Y., Yoshimoto, N., Orense, R., 2007. Shear behavior of methane hydrate-bearing sand. Proceedings of the 17th International Offshore and Polar Engineering Conference, ISOPE, pp. 1326–1333.
Kvenvolden, K.A., 1988. Methane hydrate — a major reservoir of carbon in the shallow geosphere? Chem. Geology 71 (1–3), 41–51.
Kvenvolden, K.A., Lorenson, T.D., 2001. The global occurrence of natural gas hydrate,. Geophysical Monogr. 124 (322), 3–18.
Lu, X.B., Wang, L., Wang, S.Y., Li, Q.P., 2008. Study on the mechanical properties of the tetrahydrofuran hydrate deposit. Proceedings of the 18th International Offshore and Polar Engineering Conference, ISOPE, pp. 57–60.
MacDonald, I.R., Guinasso Jr., N.L., Sassen, R., Brooks, J.M., Lee, L., Scott, K.T., 1994. Gas hydrate that breaches the sea floor on the continental slope of the Gulf of Mexico. Geological Soc. Am. 22 (8), 699–702.
Masui, A., Haneda, H., Ogata, Y., Aoki, K., 2005. The effect of saturation degree of methane hydrate on the shear strength of synthetic methane hydrate sediments. Proceedings of the 5th International Conference on Gas Hydrates (ICGH 2005), pp. 2, 657–2, 663.
Masui, A., Miyazaki, K., Haneda, H., Ogata, Y., Aoki, K., 2008. Mechanical characteristics of natural and artificial gas hydrate bearing sediments. Proceedings of the 6th International Conference on Gas Hydrates, ICGH.
Miyazaki, K., Masui, A., Haneda, H., Ogata, Y., Aoki, K., Yamaguchi, T., 2008. Variable-compliance-type constitutive model for methane hydrate bearing sediment. Proceedings of the 6th International Conference on Gas Hydrates, ICGH.
Pooladi-Darvish, M., 2004. Gas production from hydrate reservoirs and its modeling. J. Petroleum Technol. 56 (6), 65–71.
Shen, Z.J., 1993. An elasto-plastic damage model for cemented clays. Chin. J. Geotechnical Eng. 15, 21–28.
Wang, D.Y., Ma, W., Chang, X.X., 2004a. Analyses of behavior of stress–strain of frozen Lanzhou loess subjected to K_0 consolidation. Cold Regions Sci. Technol. 40, 19–29.
Wang, L.Z., Zhao, Z.Y., Li, L.L., 2004b. Non-linear elastic model considering soil structural damage. J. Hydraulic Eng. 83–89.
Winters, W.J., Pecher, I.A., Waite, W.F., Mason, D.H., 2004. Physical properties and rock physics models of sediment containing natural and laboratory-formed methane gas hydrate. Am. Mineralogist 89, 1221–1227.
Winters, W.J., Waite, W.F., Mason, D.H., Gilbert, L.Y., Pecher, I.A., 2007. Methane gas hydrate effect on sediment acoustic and strength properties. J. Petroleum Sci. Eng. 56, 127–135.
Yun, T.S., Santamarina, J.C., Ruppel, C., 2007. Mechanical properties of sand, silt, and clay containing tetrahydrofuran hydrate. J. Geophysical Res. 112 (B04106), 1–13.